

Controlling arbitrary $n \times n$ unitaries with a complete graph of $n + 1$ qubits: Beyond the single-excitation subspace

Michael R. Geller^{1,*}

¹*Department of Physics and Astronomy, University of Georgia, Athens, Georgia 30602, USA*

(Dated: October 7, 2015)

Quantum computation and simulation with a complete graph of superconducting qubits has been proposed [Phys. Rev. A **91**, 062309 (2015)]. The method does not require error correction and is practical now. By controlling the vertices (qubits) and edges (couplers) appropriately, and working in the single-excitation subspace (SES), a real but otherwise arbitrary $n \times n$ Hamiltonian can be directly programmed into the chip. The SES method, however, requires a physical qubit for every basis state in the computer's Hilbert space. This imposes large resource costs for algorithms using registers of ancillary qubits, as each ancilla doubles the required graph size. Here we show how to circumvent this doubling by leaving the SES and reintroducing a tensor product structure in the computational subspace. Specifically, we implement the tensor product of an SES register holding “data” with one or more ancilla qubits, which are able to independently control arbitrary $n \times n$ unitary operations on the data in a constant number of steps. This enables a hybrid form of quantum computation where fast SES operations are performed on the data, traditional logic gates and measurements are performed on the ancillas, and controlled-unitaries act between. As an application we give an ancilla-assisted SES implementation of the quantum linear system solver of Harrow, Hassidim, and Lloyd, and estimate that reasonably accurate symmetric matrix inversions up to dimension 10 would be possible before running out of coherence time.

PACS numbers: 03.67.Lx, 85.25.Cp

I. INTRODUCTION

The single-excitation subspace (SES) method [1, 2] uses a complete graph of n superconducting qubits and performs quantum computations and simulations in the n -dimensional SES, where the system Hamiltonian is directly programmed. This eliminates the need to decompose operations into elementary one- and two-qubit gates, allowing larger computations to be performed with the available coherence time. Symmetric $n \times n$ unitaries can be implemented in a single step, and nonsymmetric unitaries in three. The method also enables quantum simulation of n -dimensional closed systems. We call the approach *prethreshold*, referring to the threshold theorem of fault-tolerant quantum computation, because it does not require error correction.

Restriction to the SES means that a physical qubit is required for every basis state of the computational Hilbert space and the method is not scalable. A technically unscalable architecture, however, might still be useful for practical prethreshold quantum computation. But the scaling imposes large resource costs for algorithms involving ancillary qubits, as each ancilla doubles the required graph size. Here we show how to circumvent this doubling by reintroducing a tensor product structure in the computational Hilbert space, which necessitates leaving the SES. In particular, we show that a complete graph of $n + n'$ qubits can implement the tensor product of an n -qubit SES register holding “data” with n' ancilla qubits,

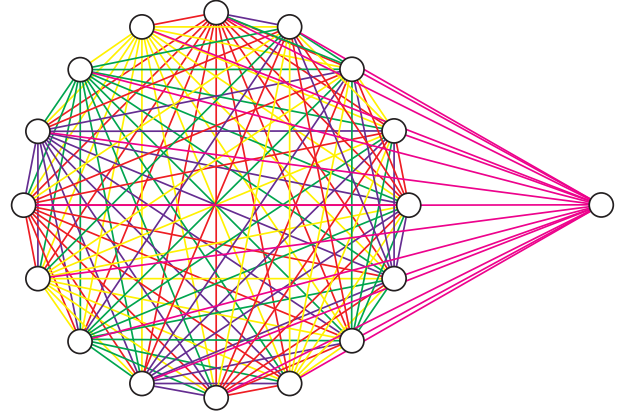


FIG. 1. (Color online) Adding a qubit to the $n = 16$ graph.

in such a way that each ancilla controls the application of an arbitrary $n \times n$ unitary to the data. In applications we will typically have n large but $n' = O(\log n)$. Crucially, the number of steps required to perform a set of n' controlled-unitaries is independent of n and only linear in n' (as they are performed serially).

To better understand the tensor product structure consider adding a single superconducting qubit to an existing SES array, resulting in a complete graph of $n + 1$ qubits; see Fig. 1. There are two distinct ways of doing this, which we call *direct sum* and *tensor product*. The direct sum means that number of excitations remains unity and the dimension of the computational subspace is increased by one, resulting in an $n + 1$ -qubit SES register. Adding n' qubits in this way increases the size of the register to

*mgeller@uga.edu

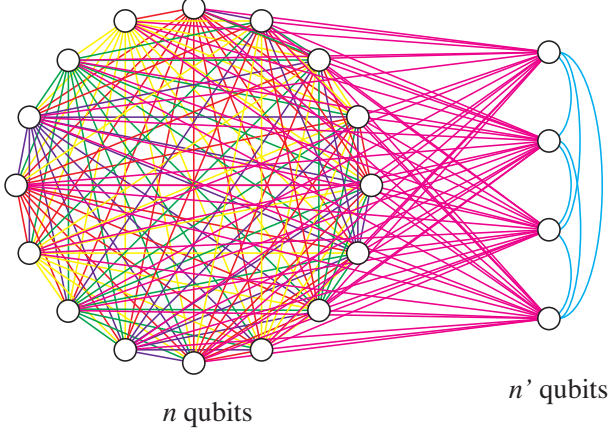


FIG. 2. (Color online) Adding a register of n' ancilla qubits creates a hybrid form of SES and gate-based computation, where fast SES operations are performed on the data, traditional logic gates and measurements are performed on the ancillas, and controlled-unitaries operate between.

$n + n'$ qubits. Or we can say we have added an n' -qubit register to the original n -qubit register. If we denote the computational subspace of an n -qubit SES register by SES_n , the direct sum implements

$$\text{SES}_n \oplus \text{SES}_{n'} = \text{SES}_{n+n'}. \quad (1)$$

The tensor product option comes from the standard model of quantum computation, where each physical qubit has a two-dimensional complex Hilbert space \mathbb{C}^2 , and the computational Hilbert space of n qubits is the tensor product $\mathbb{C}^2 \otimes \mathbb{C}^2 \otimes \dots \otimes \mathbb{C}^2$. In this paper we implement a tensor product of the form

$$\text{SES}_n \otimes \mathbb{C}^2, \quad (2)$$

which adds an excitation and is equivalent in computational subspace size to SES_{2n} . The added qubit can be used as an ancilla to control the application of arbitrary unitaries to the data stored in $|\psi\rangle \in \text{SES}_n$, enabling transformations from product states

$$|\psi\rangle \otimes (\alpha|0\rangle_{n+1} + \beta|1\rangle_{n+1}) \quad (3)$$

to arbitrary states of the form

$$\alpha (U_0|\psi\rangle) \otimes |0\rangle_{n+1} + \beta (U_1|\psi\rangle) \otimes |1\rangle_{n+1}, \quad (4)$$

which are entangled when $U_0 \neq U_1$. Here qubit $n+1$ is the ancilla. Adding n' ancilla in this manner implements

$$\text{SES}_n \otimes \underbrace{\mathbb{C}^2 \otimes \dots \otimes \mathbb{C}^2}_{n' \text{ qubits}} = \text{SES}_{n \times 2^{n'}}. \quad (5)$$

An example is given in Fig. 2. By (5) we mean that the resulting computational subspace has dimension $n \times 2^{n'}$. Because this is exponential in n' , larger problem sizes become possible.

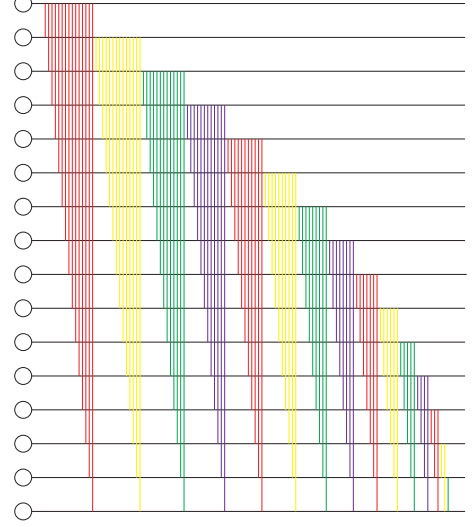


FIG. 3. (Color online) Possible layout for an SES chip. The circles are qubits and the lines are couplers.

II. CONTROLLED-UNITARY PROTOCOL

A. SES computer chip

The hardware required for ancilla-assisted SES computation is identical to that described in [1], i.e., a complete graph (fully connected array) of superconducting transmon [3] or Xmon [4] qubits with tunable frequencies and tunable $\sigma^x \otimes \sigma^x$ coupling [5]. The device Hamiltonian is

$$H_{\text{qc}} = \sum_i \begin{pmatrix} 0 & 0 \\ 0 & \epsilon_i \end{pmatrix}_i + \frac{1}{2} \sum_{ii'} g_{ii'} \sigma_i^x \otimes \sigma_{i'}^x, \quad (6)$$

with ϵ_i and $g_{ii'}$ tunable. $g_{ii'}$ is a real, symmetric matrix with vanishing diagonal elements. A possible chip layout is shown in Fig. 3.

B. SES method basics

In the SES method without ancillas [1, 2], computations are performed in the n -dimensional subspace spanned by the basis states

$$|i\rangle \equiv |0 \dots 1_i \dots 0\rangle, \quad i \in \{1, 2, \dots, n\}. \quad (7)$$

A pure state in the SES has the form

$$|\psi\rangle = \sum_{i=1}^n a_i |i\rangle, \quad \text{with} \quad \sum_{i=1}^n |a_i|^2 = 1. \quad (8)$$

The advantage of working in the SES is that the matrix elements

$$\mathcal{H}_{ii'} \equiv \langle i | H_{\text{qc}} | i' \rangle = \epsilon_i \delta_{ii'} + g_{ii'} \quad (9)$$

can be directly controlled. *Therefore we can directly program the Hamiltonian of the computer chip.*

The protocol for implementing a specific operation depends on the functionality (available ranges of the ϵ_i and $g_{ii'}$) of the SES chip. In this work we assume that the experimentally controlled SES Hamiltonian can be written, apart from an additive constant, in the *standard form*

$$\mathcal{H} = g_{\max} K \quad \text{with} \quad -1 \leq K_{ii'} \leq 1. \quad (10)$$

Here g_{\max} is the maximum interaction strength provided by the coupler circuits. A reasonable value for g_{\max}/\hbar is 50 MHz.

The basic single-step operation in SES quantum computing is the application of a symmetric unitary of the form e^{-iA} to the data, where A is a given real symmetric matrix. If only e^{-iA} is given the classical overhead for obtaining A from e^{-iA} is to be included in the quantum runtime. (Note that the generator A is not unique because the matrix logarithm is not unique.) Define

$$\theta_A \equiv \max_{ii'} |A_{ii'} - c\delta_{ii'}|, \quad (11)$$

where $c = (\min_i A_{ii} + \max_i A_{ii})/2$. The optimal SES Hamiltonian \mathcal{H} able to implement e^{-iA} (up to a phase) is given by the standard form (10), with

$$K = \frac{A - cI}{\theta_A}. \quad (12)$$

Here I is the $n \times n$ identity, and the matrix elements of (12) satisfy $|K_{ii'}| \leq 1$. The associated evolution time is

$$t_A = \frac{\hbar\theta_A}{g_{\max}}. \quad (13)$$

Additional discussion of these results is provided in Refs. [1] and [2].

Experimentally, then, the operation e^{-iA} results from evolution under the Hamiltonian H_{qc} with $\epsilon_i = \epsilon_0 + g_{\max}K_{ii}$, where ϵ_0 is a fixed qubit parking frequency, and $g_{ii'} = g_{\max}K_{ii'}$ ($i \neq i'$), for a time duration t_A . It is not even necessary for \mathcal{H} to be abruptly switched on and off: Any SES Hamiltonian of the form $\mathcal{H} = g(t)K$ such that $\int (g/\hbar) dt = \theta_A$ may be used.

C. Single-hole states

The idea underlying the controlled-unitary protocol is to use the non-SES states

$$|\bar{i}\rangle \equiv (\sigma^x)^{\otimes n} |i\rangle = |1 \cdots 10_i 1 \cdots 1\rangle, \quad (14)$$

which have $n - 1$ excitations and which are particle-hole dual to the SES basis states. The dual state $|\bar{i}\rangle$ has a single hole (absence of excitation) in qubit i . In a graph with $g_{ii'} = 0$, the basis state $|i\rangle$ is an eigenstate with energy ϵ_i , whereas $|\bar{i}\rangle$ has energy $E_n - \epsilon_i$, where

$$E_n \equiv \sum_{i=1}^n \epsilon_i \quad (15)$$

is the energy of the filled “band” $|11 \cdots 1\rangle$ of n excitations. Therefore, apart from a constant shift E_n , the dual states have *negative* energies; the resulting minus sign is the key to the protocol.

D. Description of the protocol

First we discuss the addition of a single ancilla. The objective is to implement the controlled-unitary

$$U \otimes |0\rangle\langle 0|_{n+1} + I \otimes |1\rangle\langle 1|_{n+1}, \quad (16)$$

where U is an arbitrary $n \times n$ unitary matrix acting on the SES register, and I is the $n \times n$ identity. (This definition differs from the usual one by NOT gates on the ancilla.) Partition an $n + 1$ -qubit complete graph into an n -qubit SES register and one ancilla. The initial state is of the form

$$|\psi\rangle \otimes (\alpha |0\rangle_{n+1} + \beta |1\rangle_{n+1}) \quad (17)$$

or

$$\left(\sum_{i=1}^n a_i |i\rangle \right) \otimes (\alpha |0\rangle_{n+1} + \beta |1\rangle_{n+1}). \quad (18)$$

Write the unitary in (16) in spectral form as $V e^{-iD} V^\dagger$, or equivalently

$$U = V e^{-iD/2} e^{-iD/2} V^\dagger, \quad (19)$$

where V is unitary and D is a real diagonal matrix. We will make U conditional by implementing

$$U = V e^{-iD/2} e^{\pm iD/2} V^\dagger \quad (20)$$

instead of (19), where the plus sign comes from the negative energy of the single-hole states and results in an application of the identity.

The first three steps of the protocol are to implement the V^\dagger operation in (20) on the data stored in the SES register. The ABA decomposition [2] is used to write V and V^\dagger as

$$V = e^{-iA} e^{-iB} e^{iA} \quad \text{and} \quad V^\dagger = e^{-iA} e^{iB} e^{iA}, \quad (21)$$

where A and B are real symmetric matrices. The procedure for computing A and B is given in [2]. Each operator produced by the ABA decomposition is a symmetric unitary and can be implemented in a single step (Sec. II B). The first operation, e^{iA} , results from evolution under H_{qc} with $\epsilon_i = \epsilon_0 + g_{\max}K_{ii}$ (ϵ_0 is a fixed qubit parking frequency) and $g_{i \neq i'} = g_{\max}K_{ii'}$, with $K = -(A - cI)/\theta_A$, for a time duration $t_A = \hbar\theta_A/g_{\max}$. The indices i and i' in these expressions include the SES partition $\{1, \dots, n\}$ only, and during this operation all couplings to the ancilla are turned off ($g_{i,n+1} = 0$ for all $i \in \{1, \dots, n\}$). These settings program the SES Hamiltonian $\mathcal{H} = g_{\max}K$ into the chip. The ancilla qubit frequency ϵ_{n+1} is set to ϵ_0 .

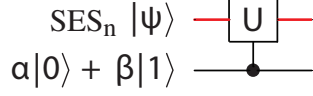


FIG. 4. (Color online) Controlled unitary operation. The red upper line is an n -qubit SES register, the black lower line is the ancilla qubit.

The protocol implements the symmetric unitary e^{iA} up to a phase, with that phase chosen to minimize t_A . e^{-iA} is implemented by changing $K \rightarrow -K$. $e^{\pm iB}$ are implemented by changing $A \rightarrow B$. The total time required to implement V^\dagger is $t_V = 2t_A + t_B$. After these steps (18) becomes

$$\left(\sum_{i=1}^n (V^\dagger a)_i |i\rangle \right) \otimes (\alpha|0\rangle_{n+1} + e^{-i\epsilon_0 t_V / \hbar} \beta|1\rangle_{n+1}), \quad (22)$$

where, for any unitary W acting on the SES, we write $\sum_{i'} \langle i|W|i'\rangle a_{i'}$ as $(Wa)_i$. Note that the ancilla acquired a relative phase after these operations; we assume that such phases are removed by applying z rotations to the ancilla or by working in a rotating frame.

The next steps apply $e^{\pm iD/2}$ conditioned on the ancilla, the sign change resulting from the negative energies of the dual states. After CNOT gates between the ancilla (control) and each of n SES qubits (targets), we have

$$\sum_{i=1}^n \left((V^\dagger a)_i |i\rangle \otimes \alpha|0\rangle_{n+1} + (V^\dagger a)_i |\bar{i}\rangle \otimes \beta|1\rangle_{n+1} \right). \quad (23)$$

In Sec. II E we show to implement these CNOT gates *simultaneously*. Then follow a protocol as if to implement the diagonal operator operator $e^{-iD/2}$ in the SES: Apply H_{qc} with $g_{ii'} = 0$ and $\epsilon_i = \epsilon_0 + g_{\max} K_{ii}$ for a time $t_D = \hbar \theta_D / 2g_{\max}$. Here $K \equiv (D - cI)/\theta_D$, $\theta_D \equiv \max_i |D_{ii} - c|$, and $c = (\min_i D_{ii} + \max_i D_{ii})/2$. Set the ancilla frequency to ϵ_0 . Following this operation, and another ancilla z rotation, (23) becomes

$$\sum_{i=1}^n \left((e^{-iD/2} V^\dagger a)_i |i\rangle \otimes \alpha|0\rangle_{n+1} + (e^{iD/2} V^\dagger a)_i |\bar{i}\rangle \otimes \beta|1\rangle_{n+1} \right).$$

After a second set of CNOT gates and subsequent application of $e^{-iD/2}$ and V to the SES, and a final ancilla z rotation, we obtain

$$\sum_{i=1}^n \left((Ua)_i |i\rangle \otimes \alpha|0\rangle_{n+1} + a_i |i\rangle \otimes \beta|1\rangle_{n+1} \right), \quad (24)$$

or

$$U|\psi\rangle \otimes \alpha|0\rangle_{n+1} + |\psi\rangle \otimes \beta|1\rangle_{n+1}, \quad (25)$$

as required. We represent this operation by the circuit diagram of Fig. 4.

Up to this point we have described the use of a single ancilla. The total number of steps required to implement the controlled unitary (about 10) is independent of n . Additional ancilla can be included by increasing the graph size by one for each new ancilla. Each ancilla independently controls unitaries acting on the shared data register. These unitaries, however, cannot be performed simultaneously, so in most applications the runtime will scale linearly with the number of ancilla n' .

E. Multi-target CNOT

The protocol of the last section requires two rounds of CNOT gates applied between the ancilla (control) and the n qubits in the SES partition (targets). For small n these can be done serially using the high-fidelity entangling gates developed for standard gate-based superconducting quantum computation. The CNOT gates commute, however, and in principal can be performed simultaneously. Multi-target CNOT gate protocols [6–13] have been developed for ion trap, cavity QED, and circuit QED architectures, where many qubits can be coupled to a common cavity or other bosonic mode. These protocols can be applied to the complete graph architecture as well, but at the expense of supplementing each ancilla with an additional resonator or qubit, which must also be fully connected. The desired tensor product would then require $n + 2n'$ qubits. We avoid this overhead by designing a fast multi-target CNOT gate specifically for the complete graph.

It is well known that the entangling gate

$$e^{-i\frac{\pi}{4}\sigma^x \otimes \sigma^x} \quad (26)$$

is *locally* equivalent to a two-qubit CNOT gate, meaning that it is a CNOT apart from single-qubit rotations. To see this, let the second qubit be the control, and apply Hadamards to obtain $e^{-i\frac{\pi}{4}\sigma^x \otimes \sigma^z}$. This operator acts with $e^{-i\frac{\pi}{4}\sigma^x}$ on the target when the control is $|0\rangle$, and with $e^{i\frac{\pi}{4}\sigma^x}$ when the control is $|1\rangle$, from which it is straightforward to construct a CNOT.

It is not surprising that a simultaneous multi-target CNOT gate is possible in the complete graph architecture, and the Hamiltonian (6) already contains an interaction underlying such an operation: Set the couplings between the ancilla and the n qubits in the SES partition to a positive constant g and all others to zero, as illustrated in Fig. 5. The interaction

$$g \left(\sum_{i=1}^n \sigma_i^x \right) \otimes \sigma_{n+1}^x \quad (27)$$

couples the ancilla qubit to a collective variable

$$S_x \equiv \sum_{i=1}^n \sigma_i^x \quad (28)$$

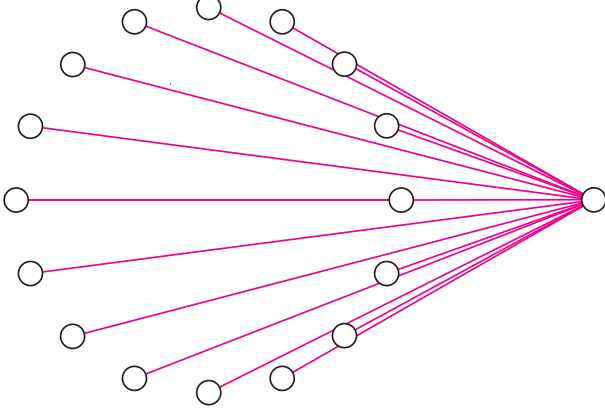


FIG. 5. (Color online) Graph to implement the n -target CNOT gate.

TABLE I. Performance of simultaneous n -target CNOT gate in complete graph of $n+1$ transmon or Xmon qubits, using realistic models for the qubits and couplers. Here η is the qubit anharmonicity, t_{gate} is the gate time excluding the single-qubit rotations in (31), Ω is the microwave Rabi frequency, and g is the coupler strength. The reported gate error is $E_{\text{gate}} \equiv 1 - |\langle \Psi | U_{\text{ideal}}^\dagger U | \Psi \rangle|^2$, where U_{ideal} is the ideal entangler (29), and U is the realized evolution operator computed in the absence of decoherence. The error is averaged over initial states $|\Psi\rangle$. The qubit frequencies are $\epsilon_0/h = 5.5$ GHz.

n	η/h	t_{gate}	Ω/h	g/h	E_{gate}
3	300 MHz	30 ns	133 MHz	8 MHz	1.7%
3	300 MHz	40 ns	100 MHz	6 MHz	1.1%
3	400 MHz	30 ns	133 MHz	8 MHz	1.1%
3	400 MHz	40 ns	100 MHz	6 MHz	0.9%
4	300 MHz	30 ns	133 MHz	8 MHz	2.8%
4	300 MHz	40 ns	100 MHz	6 MHz	2.1%
4	400 MHz	30 ns	133 MHz	8 MHz	2.2%
4	400 MHz	40 ns	100 MHz	6 MHz	1.9%

of the SES partition. Such an interaction, on its own, can be used to generate the desired multi-qubit entangling operation

$$e^{-i\frac{\pi}{4}S_x \otimes \sigma_{n+1}^x} = \prod_{i=1}^n e^{-i\frac{\pi}{4}\sigma_i^x \otimes \sigma_{n+1}^x} \quad (29)$$

that generalizes (26). The multi-target CNOT gate

$$I \otimes |0\rangle\langle 0|_{n+1} + (\sigma^x)^{\otimes n} \otimes |1\rangle\langle 1|_{n+1} \quad (30)$$

The circuit for $m = 2$ is given in Fig. 6. The central (blue) subcircuit implements the controlled-rotation

results from the pulse sequence

$$\begin{pmatrix} 1 & 0 \\ 0 & -i \end{pmatrix}_{n+1} (e^{i\frac{\pi}{4}\sigma^x})^{\otimes n} H_{n+1} e^{-i\frac{\pi}{4}S_x \otimes \sigma_{n+1}^x} H_{n+1}, \quad (31)$$

where H is the single-qubit Hadamard gate.

The device Hamiltonian (6), however, contains single-qubit terms that do not commute with (27). Therefore it will be necessary follow a modified protocol to obtain the entangler (29): Add a σ^x microwave drive to the ancilla and transform to the usual rotating frame, where the $\sigma^x \otimes \sigma^x$ interaction becomes $\frac{1}{2}(\sigma^x \otimes \sigma^x + \sigma^y \otimes \sigma^y)$, and then transform to a second rotating frame where the interaction is $\frac{1}{2}\sigma^x \otimes \sigma^x$. This is discussed further in Appendix A.

Finally, we discuss the expected performance of this design when implemented in a transmon-based chip with inductive couplers. The main source of error is leakage into higher lying $|2\rangle$ states neglected in (6) but present in a real device. Although the current design has not been optimized to minimize this leakage, the estimated performance is already satisfactory for initial demonstrations, as indicated in Table I.

III. APPLICATION TO MATRIX INVERSION

As an application of these techniques we give an ancilla-assisted SES implementation of the quantum linear system solver of Harrow, Hassidim, and Lloyd [14]. We choose this algorithm because it requires a large register of ancilla qubits, which is challenging, and because it has interesting generalizations and applications; we do not expect an SES chip running this implementation to outperform a classical supercomputer.

The matrix inversion algorithm [14, 15] solves the linear system $A\mathbf{x} = \mathbf{b}$ for \mathbf{x} , accepting \mathbf{b} in the form of a normalized pure state $|\mathbf{b}\rangle$, and returning the solution in the form of a pure state $|\mathbf{x}\rangle$. In the SES implementation these states are stored in a data register of Hilbert space dimension n . (Note that in our notation A is $n \times n$, not $2^n \times 2^n$.) A second register of m qubits is used for the phase estimation subroutine, and one more is used for postselection. The value of m determines the accuracy of the solution. The SES implementation (for symmetric A) requires a complete graph of $n + m + 1$ qubits.

operation

$$\sum_{k=0}^{2^m-1} |k\rangle\langle k| \otimes R_y(\gamma_k), \quad \gamma_k \equiv \begin{cases} 2 \arcsin(\frac{1}{k}) & \text{for } k > 0, \\ 0 & \text{for } k = 0. \end{cases} \quad (32)$$

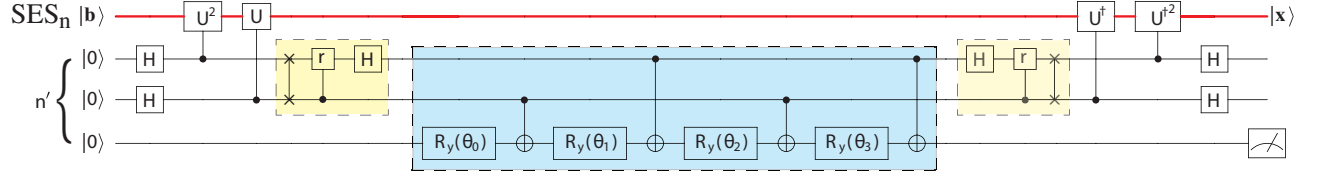


FIG. 6. (Color online) Quantum circuit for $n \times n$ matrix inversion with $m = 2$. Here H is the Hadamard gate, $U \equiv e^{iAt_0/2^m}$, the vertical line connecting crosses is a SWAP gate, $r \equiv |0\rangle\langle 0| + i|1\rangle\langle 1|$ is a z rotation, and $R_y \equiv e^{-i(\theta/2)\sigma^y}$ is a y rotation. The small (yellow) subcircuits are the Fourier transforms and the central (blue) subcircuit implements the controlled ancilla rotation (32).

Here $|k\rangle$ is a computational basis state of the m -qubit ancilla register. The rotation angles $\theta_0, \dots, \theta_3$ in Fig. 6 are determined by finding the net y rotation applied to the last qubit in each of the cases $|k\rangle \in \{|00\rangle, |01\rangle, |10\rangle, |11\rangle\}$, making use of the identity $\sigma^x R_y(\theta) \sigma^x = R_y(-\theta)$, and comparing the result with (32), rewritten as

$$\begin{aligned} &|00\rangle\langle 00| \otimes R_y(\gamma_0) + |01\rangle\langle 01| \otimes R_y(\gamma_1) \\ &+ |10\rangle\langle 10| \otimes R_y(\gamma_2) + |11\rangle\langle 11| \otimes R_y(\gamma_3). \end{aligned} \quad (33)$$

This leads to

$$\begin{pmatrix} 1 & 1 & 1 & 1 \\ 1 & -1 & -1 & 1 \\ 1 & 1 & -1 & -1 \\ 1 & -1 & 1 & -1 \end{pmatrix} \begin{pmatrix} \theta_0 \\ \theta_1 \\ \theta_2 \\ \theta_3 \end{pmatrix} = \begin{pmatrix} \gamma_0 \\ \gamma_1 \\ \gamma_2 \\ \gamma_3 \end{pmatrix}, \quad (34)$$

with the γ_k given in (32). The matrix in (34), after multiplication by $2^{-m/2}$, is orthogonal and hence immediately inverted, yielding the θ_k .

The $m = 2$ phase estimation is not sufficiently accurate for matrix inversion, typically leading to 5-15% algorithm errors for matrix sizes $2 \leq n \leq 4$. By algorithm error we mean

$$E_{\text{algorithm}} \equiv 1 - \langle \mathbf{x}_{\text{ideal}} | \rho_{\text{data}} | \mathbf{x}_{\text{ideal}} \rangle, \quad (35)$$

where ρ_{data} is the final state of the data register, traced over the $m + 1$ ancilla, and $|\mathbf{x}_{\text{ideal}}\rangle$ is the pure state corresponding to the exact solution of the given linear system. The circuit of Fig. 6 can be easily extended to larger m , however, and the performance for $m = 3$ is already quite good. The controlled-rotation subcircuit for $m > 2$ can be obtained from the “uniformly controlled rotation” operator construction of Möttönen *et al.* [16], which requires 2^m CNOT gates (and is therefore not useful for large m). Simulating the $m = 3$ circuit we find that real symmetric matrices up to dimension 10 can be inverted with algorithm errors less than 5%, as shown in Fig. 7, a considerable increase in problem size over the existing gate-based realizations [17–19].

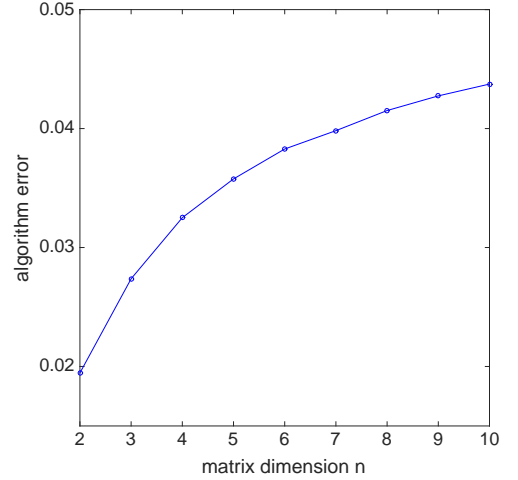


FIG. 7. (Color online) Matrix inversion algorithm error for $m = 3$, averaged over random real symmetric matrices A (with eigenvalues $0 < \lambda_i < 1$). The error computed here results from the low precision of the phase estimation procedure (small m value) only and does not include the effects of decoherence and other errors that would arise during implementation.

ACKNOWLEDGMENTS

This work was supported by the National Science Foundation under CDI grant DMR-1029764. It is a pleasure to thank Amara Katarbwa for useful discussions.

Appendix A: Multi-qubit entangler design

In this Appendix we show how to produce the entangler (29) used to construct the multi-target CNOT gate. With the couplings between the ancilla and the n qubits in the SES partition set to a positive constant g (see

Fig. 5), the device Hamiltonian becomes

$$H = \sum_{i=1}^{n+1} \begin{pmatrix} 0 & 0 \\ 0 & \epsilon_0 \end{pmatrix}_i + g \sum_{i=1}^n \sigma_i^x \otimes \sigma_{n+1}^x + \Omega \cos\left(\frac{\epsilon_0 t}{\hbar}\right) \sigma_{n+1}^x, \quad (\text{A1})$$

where we have added a resonant microwave drive to the ancilla. Decompose the time evolution operator generated by (A1) as

$$U = e^{-iD_a t/\hbar} U_a, \quad \text{with } D_a \equiv \sum_{i=1}^{n+1} \begin{pmatrix} 0 & 0 \\ 0 & \epsilon_0 \end{pmatrix}_i. \quad (\text{A2})$$

Then $\dot{U}_a = -iH_a U_a$, where

$$H_a \approx \frac{g}{2} \sum_{i=1}^n \left(\sigma_i^x \otimes \sigma_{n+1}^x + \sigma_i^y \otimes \sigma_{n+1}^y \right) + \frac{\Omega}{2} \sigma_{n+1}^x \quad (\text{A3})$$

is the Hamiltonian in the z -rotating frame. We choose the evolution time to satisfy

$$t_{\text{gate}} = l_a \left(\frac{2\pi\hbar}{\epsilon_0} \right), \quad (\text{A4})$$

where l_a is an integer, which makes the small corrections to (A3) vanish when averaged over t_{gate} , and also makes $e^{-iD_a t/\hbar} = I$. The value of l_a (usually between 100 and 300) is determined by the desired gate time.

Next decompose U_a as

$$U_a = e^{-iD_b t/\hbar} U_b, \quad \text{with } D_b \equiv \frac{\Omega}{2} \sigma_{n+1}^x. \quad (\text{A5})$$

Then $\dot{U}_b = -iH_b U_b$, where

$$H_b \approx \frac{g}{2} \sum_{i=1}^n \sigma_i^x \otimes \sigma_{n+1}^x = \frac{g}{2} S_x \otimes \sigma_{n+1}^x \quad (\text{A6})$$

is the Hamiltonian in a second frame rotating the ancilla about the x axis. We choose the Rabi frequency to satisfy

$$\Omega = l_b \left(\frac{4\pi\hbar}{t_{\text{gate}}} \right), \quad (\text{A7})$$

where l_b is another integer, which makes the corrections to (A6) vanish on average and also makes $e^{-iD_b t/\hbar} = \pm I$. The value of l_b is chosen to minimize the total gate error: When $l_b = 1$ the corrections to (A6) are significant and lead to undesirable errors, but when l_b is larger the microwave field causes leakage. We find that $l_b = 2$ is optimal. The effect of this second transformation is to remove the $\sigma^y \otimes \sigma^y$ term in (A6). Note the factor of $\frac{1}{2}$ in (A6) that is not present in (A1).

With these parameters the evolution operator becomes

$$U \approx e^{-i\frac{g}{2} S_x \otimes \sigma_{n+1}^x t_{\text{gate}}}. \quad (\text{A8})$$

Setting the coupling strength to $g = \pi\hbar/2t_{\text{gate}}$ generates the desired entangler (29).

-
- [1] M. R. Geller, J. M. Martinis, A. T. Sornborger, P. C. Stancil, E. J. Pritchett, H. You, and A. Galiatdinov, *Phys. Rev. A* **91**, 062309 (2015).
 - [2] A. Katabarwa and M. R. Geller, *Phys. Rev. A* **92** (2015).
 - [3] J. Koch, T. M. Yu, J. Gambetta, A. A. Houck, D. I. Schuster, J. Majer, A. Blais, M. H. Devoret, S. M. Girvin, and R. J. Schoelkopf, *Phys. Rev. A* **76**, 042319 (2007).
 - [4] R. Barends, J. Kelly, A. Megrant, D. Sank, E. Jeffrey, Y. Chen, Y. Yin, B. Chiaro, J. Mutus, C. Neill, P. O'Malley, P. Roushan, J. Wenner, T. C. White, A. N. Cleland, and J. M. Martinis, *Phys. Rev. Lett.* **111**, 080502 (2013).
 - [5] Y. Chen, C. Neill, P. Roushan, N. Leung, M. Fang, R. Barends, J. Kelly, B. Campbell, Z. Chen, B. Chiaro, A. Dunsworth, E. Jeffrey, A. Megrant, J. Y. Mutus, P. J. J. O'Malley, C. M. Quintana, D. Sank, A. Vainsencher, J. Wenner, T. C. White, M. R. Geller, A. N. Cleland, and J. M. Martinis, *Phys. Rev. Lett.* **113**, 220502 (2014).
 - [6] X. Wang, A. Sørensen, and K. Mølmer, *Phys. Rev. Lett.* **86**, 3907 (2001).
 - [7] C.-P. Yang and S. Han, *Phys. Rev. A* **72**, 032311 (2005).
 - [8] X.-M. Lin, Z.-W. Zhou, M.-Y. Ye, Y.-F. Xiao, and G.-C. Guo, *Phys. Rev. A* **73**, 012323 (2006).
 - [9] C.-P. Yang, Y.-X. Liu, and F. Nori, *Phys. Rev. A* **81**, 062323 (2010).
 - [10] M. Waseem, M. Irfan, and S. Qamar, *Physica C* **477**, 24 (2012).
 - [11] K.-H. Song, Z.-G. Shi, S.-H. Xiang, and X.-W. Chen, *Physica B* **407**, 3596 (2012).
 - [12] C.-P. Yang, Q.-P. Su, F.-Y. Zhang, and S.-B. Shi-Biao Zheng, *Optics Letters* **39**, 3312 (2014).
 - [13] X. Liu, G.-Y. Fang, Q.-H. Liao, and S.-T. Liu, *Phys. Rev. A* **90**, 062330 (2014).
 - [14] A. W. Harrow, A. Hassidim, and S. Lloyd, *Phys. Rev. Lett.* **103**, 150502 (2009).
 - [15] B. D. Clader, B. C. Jacobs, and C. R. Sprouse, *Phys. Rev. Lett.* **110**, 250504 (2013).
 - [16] M. Möttönen, J. J. Vartiainen, V. Bergholm, and M. M. Salomaa, *Phys. Rev. Lett.* **93**, 130502 (2004).
 - [17] X.-D. Cai, C. Weedbrook, Z.-E. Su, M.-C. Chen, M. Gu, M.-J. Zhu, L. Li, N.-L. Liu, C.-Y. Lu, and J.-W. Pan, *Phys. Rev. Lett.* **110**, 230501 (2013).
 - [18] J. Pan, Y. Cao, X. Yao, Z. Li, C. Ju, H. Chen, X. Peng, S. Kais, and J. Du, *Phys. Rev. A* **89**, 022313 (2014).
 - [19] S. Barz, I. Kassal, M. Ringbauer, Y. O. Lipp, B. Dakić, A. Aspuru-Guzik, and P. Walther, *Sci. Rep.* **4**, 6115 (2014).